High-speed solar wind stream effects on the topside ionosphere over Arecibo: A case study during solar minimum

Rajkumar Hajra, Bruce T. Tsurutani, Christiano G. M. Brum, Ezequiel Echer

AGU PUBLICATIONS

Geophysical Research Letters

RESEARCH LETTER
10.1002/2017GL073805

Key Points:
- Impact of an interplanetary high-speed solar wind stream (HSS) on the near-equatorial topside ionosphere is studied for the first time
- The topside ionosphere expanded in altitude (100-200 km) and became hotter (50–500 K) during the HSS
- The electron density of the topside ionosphere increased by a factor of ~4 during the HSS compared to a non-HSS interval

Correspondence to:
R. Hajra,
rajkumarhajra@yahoo.co.in

Citation:
Hajra, R., B. T. Tsurutani, C. G. M. Brum, and E. Echer (2017), High-speed solar wind stream effects on the topside ionosphere over Arecibo: A case study during solar minimum, *Geophys. Res. Lett.*, *44*, 7607–7617, doi:10.1002/2017GL073805.

Received 12 APR 2017
Accepted 24 JUL 2017
Accepted article online 28 JUL 2017
Published online 11 AUG 2017

High-speed solar wind stream effects on the topside ionosphere over Arecibo: A case study during solar minimum

Rajkumar Hajra[1], Bruce T. Tsurutani[2], Christiano G. M. Brum[3], and Ezequiel Echer[4]

[1]Laboratoire de Physique et Chimie de l'Environnement et de l'Espace, CNRS, Orléans, France, [2]Jet Propulsion Laboratory, California Institute of Technology, Pasadena, California, USA, [3]Space and Atmospheric Science Department, Arecibo Observatory/SRI International, Arecibo, Puerto Rico, [4]Instituto Nacional de Pesquisas Espaciais, São José dos Campos, Brazil

Abstract The impact of a high-speed solar wind stream (HSS) on the topside near-equatorial ionosphere (Arecibo: 28.17°N, L = 1.3) is investigated for the first time. Although the HSS did not lead to any significant geomagnetic storm activity, the ionosphere over Arecibo became hotter and expanded significantly in altitude as compared to a non-HSS interval. The O^+/H^+ transition height h_T increased by ~200 km in the daytime and by ~100 km at night. At the h_T, the peak ionospheric electron and ion temperatures increased by ~200–500 K during day and by ~50–70 K at night. While the O^+ ion concentration exhibited an overall enhancement, deep penetration of the H^+ ions below h_T are observed during the day. The noontime peak electron density was ~4 times higher during the HSS event compared to the non-HSS interval. We present three possible mechanisms to explain this topside ionospheric heating.

1. Introduction

The topside ionosphere, extending from the *F* layer peak (~200 km) up to the protonosphere (~3000 km), mainly consists of oxygen (O^+), hydrogen (H^+), and helium (He^+) ions. The transition altitude or the base of the protonosphere, where $[O^+] = [H^+] + [He^+]$, is an important characteristic parameter of the topside ionosphere [*Titheridge*, 1976; *MacPherson et al.*, 1998; *Heelis et al.*, 2009; *Aponte et al.*, 2013; *Kotov et al.*, 2015]. In the above $[X]$ indicates the number density of X species. The transition is known to be a highly dynamic region that is sensitive to the variations of solar ionizing EUV flux and thermospheric neutral winds [e.g., *Miyazaki*, 1979; *Heelis and Hanson*, 1980; *Antonova et al.*, 1992; *González et al.*, 2004; *Heelis et al.*, 2009; *Garzón et al.*, 2011; *Aponte et al.*, 2013]. Most of the above references deal with climatological behavior of the topside ionosphere focusing on solar activity and seasonal variations.

The goal of the present effort is to study the low-latitude or near-equatorial topside ionospheric response to an interplanetary high-speed solar wind stream (HSS), or to "external solar wind forcing." The HSSs emanate from solar coronal holes [*Krieger et al.*, 1973; *Sheeley et al.*, 1976]. The HSSs interact with slow-speed solar wind streams near the ecliptic plane, giving rise to compressed plasma and magnetic field regions. These appear to corotate with the Sun and are thus called corotating interaction regions (CIRs) [*Smith and Wolfe*, 1976; *Tsurutani et al.*, 1995]. The CIRs and the following HSSs carry interplanetary Alfvén wave trains [*Belcher and Davis*, 1971; *Tsurutani et al.*, 1994]. The southward component of the Alfvén waves causes sporadic magnetic reconnection at the Earth's dayside magnetopause [*Dungey*, 1961; *Tsurutani and Gonzalez*, 1987; *Tsurutani et al.*, 1995], leading to substorms and convection events and energetic ~10–100 keV particle injections into the nightside magnetosphere [*DeForest and McIlwain*, 1971; *Horne and Thorne*, 1998].

In the present work we will explore the incoherent scatter radar (ISR) observations of the topside (~250–1300 km) ionosphere at the Arecibo Observatory situated at a near-equatorial region (geomagnetic: 28.17°N, 5.88°E, dip: 46.7°, L = 1.3) during a HSS event. We will characterize the perturbations of the topside ionosphere caused by this external (solar wind) driving. We believe that this is the first explicit study on the effect of HSSs on the topside ionosphere.

2. Data Analyses and Results

The ionospheric ISR measurements at Arecibo Observatory are available since 1988 on a campaign basis. For theoretical details of the ISR and methods of data extraction, we refer the readers to *Gordon* [1964], *Farley*

[1970], and *González and Sulzer* [1996]. From this database, only one interval with suitable measurements when a HSS hit the Earth was found. This was the HSS event during 4–8 April 2008. A "quiet period" with no HSS is selected as a reference interval for comparison to the HSS event. The quiet interval selected is 24–26 March 2009. To ensure that the non-HSS interval would be a good baseline for comparison to the HSS interval, we selected the interval to be in the same season (spring equinox) and the same average $F_{10.7}$ solar flux (solar activity conditions). The $F_{10.7}$ was 69.4 solar flux unit/sfu (1 sfu = 10^{-22} W m^{-2} Hz^{-1}) during the non-HSS and ~70.5 sfu during the HSS interval (http://www.drao.nrc.ca/icarus).

2.1. Topside Ionosphere During a Non-HSS Period: 24–26 March 2009

Figure 1 shows the solar wind/interplanetary variations along with associated ionospheric conditions during the non-HSS interval of 24–26 March 2009 (83–85 days of year/DOY 2009). The solar wind and interplanetary data at ~1 AU are obtained from the OMNI database (http://omniweb.gsfc.nasa.gov/). The peak solar wind speed V_{sw} during the interval was ~480 km s^{-1}, indicating a moderate/slow-speed solar wind stream (Figure 1a). The variations of solar wind plasma density N_{sw} (peak ~7 cm^{-3}), ram pressure P_{sw} (~2 nPa), plasma temperature T_{sw} (~3 × 10^5 K), interplanetary magnetic field (IMF) magnitude B_o (~7 nT), and B_z component (−6 nT) indicate a moderate solar wind/interplanetary condition. Figure 1e shows the high-resolution (1 min) symmetric ring current index *SYM-H* obtained from the World Data Center for Geomagnetism, Kyoto, Japan (http://wdc.kugi.kyoto-u.ac.jp/). The auroral electrojet (*SME*, Figure 1f) and its westward component (*SML*, Figure 1g) are constructed from ground magnetometer data from the SuperMAG network (http://supermag.jhuapl.edu/), the latter consisting of more than 300 ground-based magnetometers [*Gjerloev*, 2009; *Newell and Gjerloev*, 2011]. The variations of the *SYM-H* (peak −31 nT), *SME* (895 nT), and *SML* (−681 nT) indices indicate moderate geomagnetic activity condition. No magnetic storms were in progress [e.g., *Gonzalez et al*., 1994].

Figures 1h–1m display the topside ionosphere characteristics from ~1230 LT on 24 March to ~0700 LT on 26 March. From ~300 km, the electron density Ne decreases with increase in altitude (Figure 1h). At ~300 km, the Ne variation is characterized by a minimum of ~3 × 10^4 cm^{-3} around 0600 LT followed by a gradual increase until it attains a peak of ~3 × 10^5 cm^{-3} at ~1600 LT before local sunset. After sunset Ne decreases at a faster rate. At ~400 km, the minimum and peak densities are ~1.7 × 10^4 cm^{-3} and ~1.9 × 10^5 cm^{-3}, respectively. Above the *F* layer peak, collisional losses of the electrons are insignificant owing to the lower concentration of neutral molecular species. Thus, the ionospheric plasma distribution is mainly controlled by diffusion [e.g., *MacPherson et al*., 1998].

The diurnal profile of O^+ (Figure 1j) resembles that of Ne as described above. At an altitude of ~400 km, the O^+ exhibits a diurnal peak of ~1.8 × 10^5 cm^{-3} at ~1600 LT and a minimum of ~1.4 × 10^4 cm^{-3} at ~0600 LT. Above 400 km, O^+ decreases gradually. The lighter ion H^+ is dominant in the protonosphere above ~450 km at night (Figure 1i). The peak H^+ concentration of ~1–2 × 10^4 cm^{-3} is recorded at local midnight at an altitude of ~620 km.

During the present (2008–2009) solar minimum case, the He^+ ion concentration is very low compared to those of H^+ and O^+ ions [see *Aponte et al*., 2013]. As a consequence, the transition height h_T is essentially equivalent to the height where [O^+] ~ [H^+] (Figure 1k). h_T varies from a peak of ~950 km at 1245 LT (noontime peak) on 24 March to a minimum of ~430 km recorded at 0447 LT (presunrise minimum) on 25 March. The red curve in Figure 1k shows the variation of the H^+ peak altitude h_H, which is always higher than h_T under the present condition.

The electron and ion temperatures T_e and T_i at different altitudes from 400 km to 1200 km are shown in Figures 1l and 1m, respectively. During daytime, T_e and T_i have virtually the same values. At h_T, T_e, and T_i exhibit their minimum values of ~700 K at the postmidnight hour (~0200 LT). After ~0530 LT the temperatures increase gradually with time until they reach a peak of ~2500 K at ~0930 LT. The early morning period corresponds to low ionospheric plasma densities. The corresponding ionospheric temperature increases are attributed to photoelectron heating. The temperatures remain more or less constant until ~1630 LT, after which they decrease gradually.

2.2. Topside Ionosphere During a HSS Event: 4–8 April 2008

Figure 2 shows the solar wind/interplanetary and ionospheric variations associated with a HSS event occurring on 4–8 April 2008 (95–99 DOY 2008). The HSS emanated from a large solar coronal hole with positive

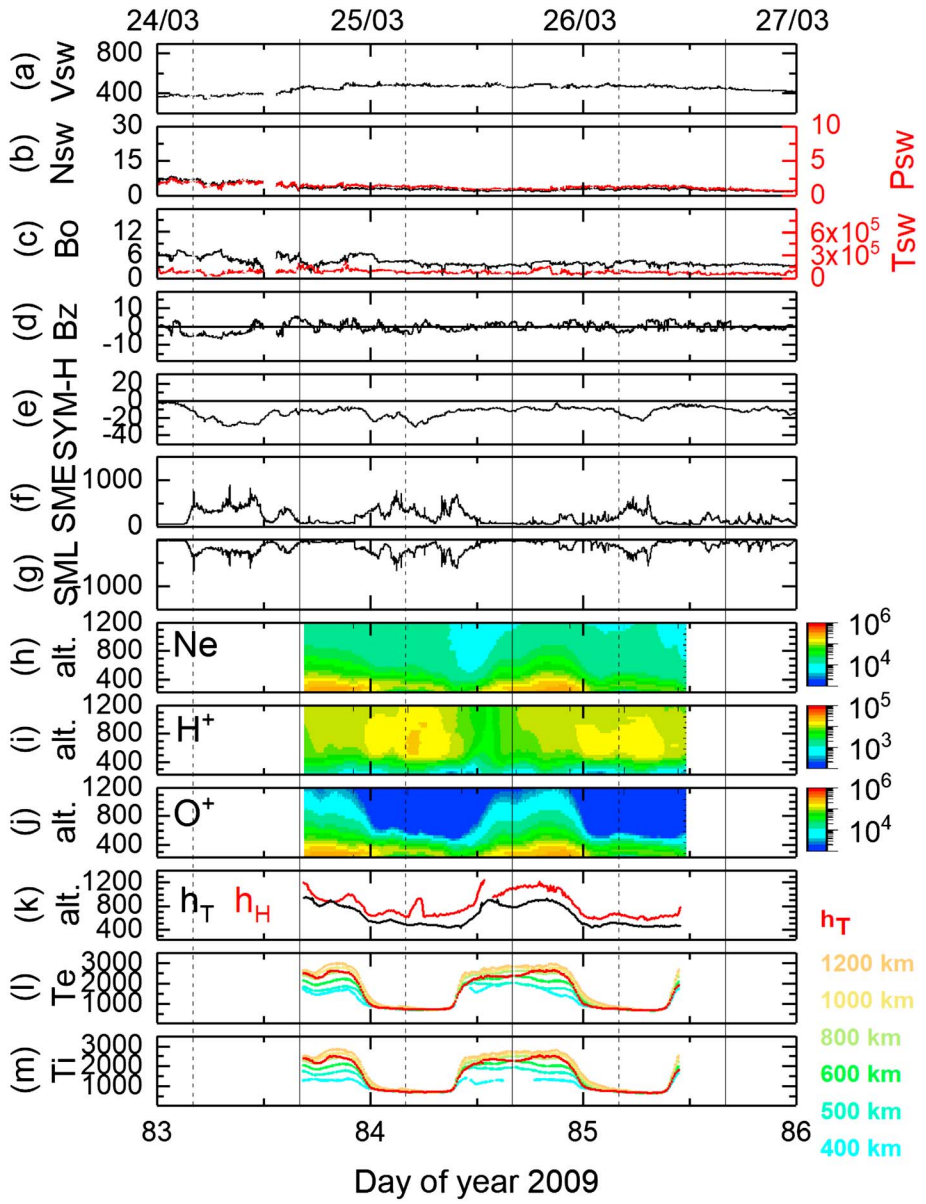

Figure 1. A non-HSS interval during 24–26 March 2009. From top to bottom, the panels show (a) V_{sw} (km s^{-1}), (b) N_{sw} (cm^{-3}, black) and P_{sw} (nPa, red), (c) IMF B_o (nT, black) and T_{sw} (K, red), (d) IMF B_z (nT), (e) *SYM-H* (nT), (f) *SME* (nT), (g) *SML* (nT), altitudinal distributions of (h) Ne (cm^{-3}), (i) H^+ concentration (cm^{-3}), and (j) O^+ concentration (cm^{-3}), (k) h_T (km, black) and h_H (km, red), and (l) T_e (K) and (m) T_i (K) at different altitudes shown on the right. In the Ne, H^+, and O^+ density panels the color bars on the right gives the concentrations (in cm^{-3}). The altitude is in the unit of kilometers, and the time is in UT. The Arecibo local midnight (0000 LT) and noon (1200 LT) times are marked by vertical dashed and solid lines, respectively (LT = UT − 4 h).

magnetic polarity (the magnetic field points away from the Sun). The coronal hole extended from ~ −25° to ~ −40° latitude around Carrington longitude ~115°–150° [see *Echer et al.*, 2011]. The HSS interacts with a slow-speed stream with a V_{sw} of ~400 km s^{-1} on 4 April (Figure 2a). The CIR is present approximately from ~1247 UT on 4 April to ~0340 UT on 5 April. The CIR is characterized by a peak N_{sw} of ~16 cm^{-3}, P_{sw} ~8 nPa, IMF B_o ~12 nT, T_{sw} ~4 × 10^5 K, and IMF B_z ~ −14 nT. The CIR is followed by the HSS proper interval. The HSS has multiple peaks of ~650 km s^{-1} at ~0458 UT on 5 April, ~740 km s^{-1} at ~0937 UT on 6 April, and ~770 km s^{-1} at ~1840 UT on 8 April. The HSS proper is associated with an Alfvén wave train that is identified by IMF B_z fluctuations that oscillate between +8 nT and −7 nT (Figure 2d).

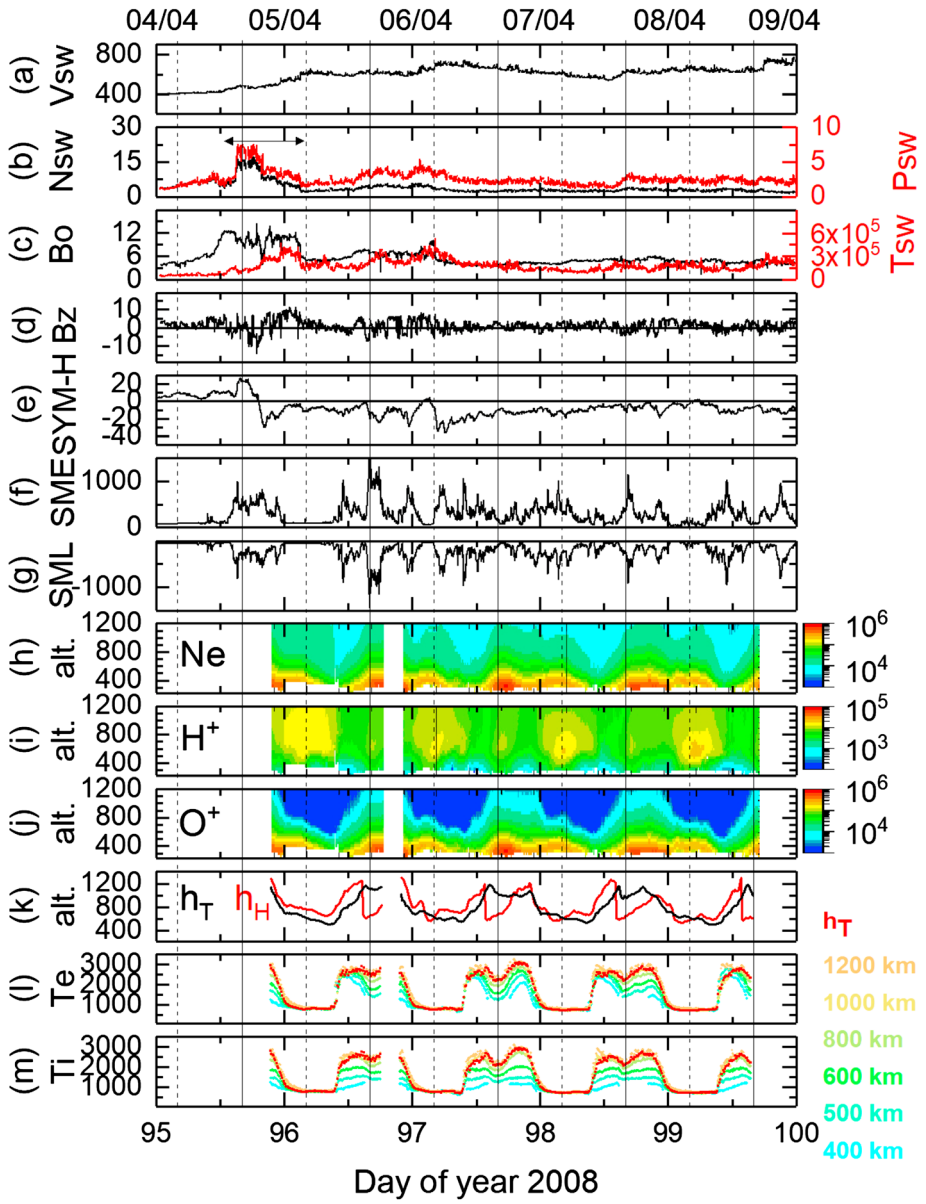

Figure 2. A HSS event on 4–8 April 2008. The panels are in the same format as in Figure 1. The horizontal arrow in Figure 2b shows the CIR interval.

The CIR/HSS event did not lead to a geomagnetic storm as defined by *Gonzalez et al*. [1994]. The variations of the *SYM-H* index (−36 nT, Figure 2e), sporadic enhancements in the *SME* (~1200 nT, Figure 2f), and *SML* (~ − 1200 nT, Figure 2g) are indicative of moderate geomagnetic activity such as substorms and convection events [*Akasofu*, 1964; *Rostoker et al*., 1980; *Newell and Gjerloev*, 2011; *Tsurutani et al*., 2004, 2015; *Hajra et al*., 2016]. The geomagnetic condition during this HSS interval is quite comparable to that during the non-HSS interval depicted in Figure 1.

The topside ionosphere measurements, from ~1730 LT on 4 April to ~1145 LT on 8 April, are shown in Figures 2h–2m. The period corresponds to the HSS proper interval after the passage of the CIR. Unfortunately, measurements are not available during the CIR impact. During the HSS proper interval, the ionosphere is observed to expand in altitude compared to quiet time (Figure 1). The electron density Ne attains a diurnal peak of ~3.9×10^5 cm^{-3} during the local noon (~1300 LT) at an altitude of ~400 km (Figure 2h). The diurnal peak occurs ~3 h earlier and is ~2 times larger than that during the non-HSS

period at 400 km altitude (Figure 1h). During this HSS interval, another secondary Ne enhancement of ~2.8 × 10^5 cm^{-3} is detected at ~2100 LT. The diurnal minimum of Ne is ~3.9 × 10^4 cm^{-3} recorded at ~0600 LT.

The O^+ variation is well correlated to the Ne variation. At 400 km altitude, the diurnal peak and minimum O^+ densities are ~3.8 × 10^5 cm^{-3} and ~2.7 × 10^4 cm^{-3}, respectively (Figure 2j). Above ~450 km, the O^+ concentration decreases gradually and H^+ dominates the nighttime protonosphere (Figure 2i). Around local midnight, H^+ has a peak concentration of ~1–2 × 10^4 cm^{-3} at an altitude of ~570 km.

The diurnal minimum of the transition height h_T is located at ~500–530 km, while the peak is at ~1150–1180 km (Figure 2k, black curve). The minimum and maximum occur near local presunrise and noon hours, respectively. The H^+ peak altitude h_H (Figure 2k, red curve) shows an interesting feature during the HSS interval. During daylight hours, ~1–1.5 h before local noon, h_H falls below the h_T. This is due to the fact that an H^+ layer with a concentration of ~10^4 cm^{-3} is formed at the altitude of ~570–600 km. The formation of additional H^+ below h_T during day when the O^+ concentration is high may have its origin in the charge exchange reaction: $O^+ + H \leftrightarrow O + H^+$ [e.g., *Garzón et al.*, 2011].

Figures 2l and 2m show the altitude variations of the electron and ion temperatures T_e and T_i, respectively. At h_T, the postmidnight minima of the ionospheric temperatures are ~750–770 K. Both T_e and T_i increase gradually after 0530 LT. T_e and T_i attain peak values of ~2800 K and ~2700 K, at ~0930 LT, respectively. T_e and T_i exhibit secondary maxima of ~3000 K at ~1630 LT, after which they decrease gradually.

In Figure 3 we compare different ionospheric parameters between the HSS (4–8 April 2008) and non-HSS (24–26 March 2009) intervals. The significantly higher values, as discussed above, are noted during the HSS event. The maximum and minimum h_T are ~200 km and ~100 km (respectively) higher during the HSS event. At h_T, the ionospheric temperatures during the HSS event are ~200–500 K higher during day and ~50–70 K higher at night as compared to the non-HSS interval. Thus, the ionosphere is warmer both during daytime and at night during the HSS interval at h_T.

Figure 4 shows a comparison of the average altitude profiles of Ne, H^+, O^+, Te, and Ti at local postmidnight (0200 LT) and afternoon (1600 LT) between the HSS and non-HSS intervals. The altitude profiles clearly indicate larger electron and ion concentrations and ionospheric temperatures during the HSS interval compared to the non-HSS interval. On average, the daytime and nighttime peak Ne densities are ~4 and ~3 times higher during the HSS event. Above ~450 km, the gradual decrease of O^+ and dominance of H^+ are clear. Large differences in T_e and T_i between the two intervals at altitudes above ~600 km reveal topside ionospheric heating by the HSS.

Figure 5 shows the geomagnetic activity data during the HSS event on 4–8 April 2008. The dynamic spectra of the ground-based magnetometer (H component) measurements are obtained from the Finnish observatory chain (~65°–69°N geographic, L ~ 4.5–5.9) (http://www.sgo.fi/Data/archive.php). The strong magnetic pulsations observed in the frequency range of 0.1–2.0 Hz represent electromagnetic ion cyclotron (EMIC) waves [*Cornwall*, 1965; *Kennel and Petschek*, 1966; *Remya et al.*, 2014, 2015, 2017]. The EMIC waves are most prominent during noon to postmidnight on 4 April, midnight to noon on 5–6 April, and on 6–7 April. It is interesting to note that the wave outbursts are well-correlated to the southward excursions in the IMF B_z (Figure 5c) and the sporadic impulses in the *SME* and *SML* indices (Figures 5e and 5f).

3. Discussion and Conclusions

We report, for the first time, HSS impacts on the near-equatorial (Arecibo Observatory, geomagnetic: 28.17°N, 5.88°E, dip: 46.7°, L = 1.3) topside ionosphere (above the *F* layer). This was compared with the topside ionospheric condition during a non-HSS interval when the seasonal and solar flux conditions were nearly the same as that for the HSS interval.

The 2008–2009 interval was characterized by the low number of equatorial and low-latitude coronal holes, low IMF magnitudes, low solar wind speed and pressure, and low-energy transfer from solar wind to the magnetosphere [*de Toma*, 2010, 2012; *Tsurutani et al.*, 2011; *Echer et al.*, 2012; *Hajra et al.*, 2013]. It was part of the prolonged solar minimum phase of the solar cycle 23, when the Sun remained at a diminished radio flux (and sunspot) level of activity. The thermosphere and ionosphere during this extreme solar minimum were

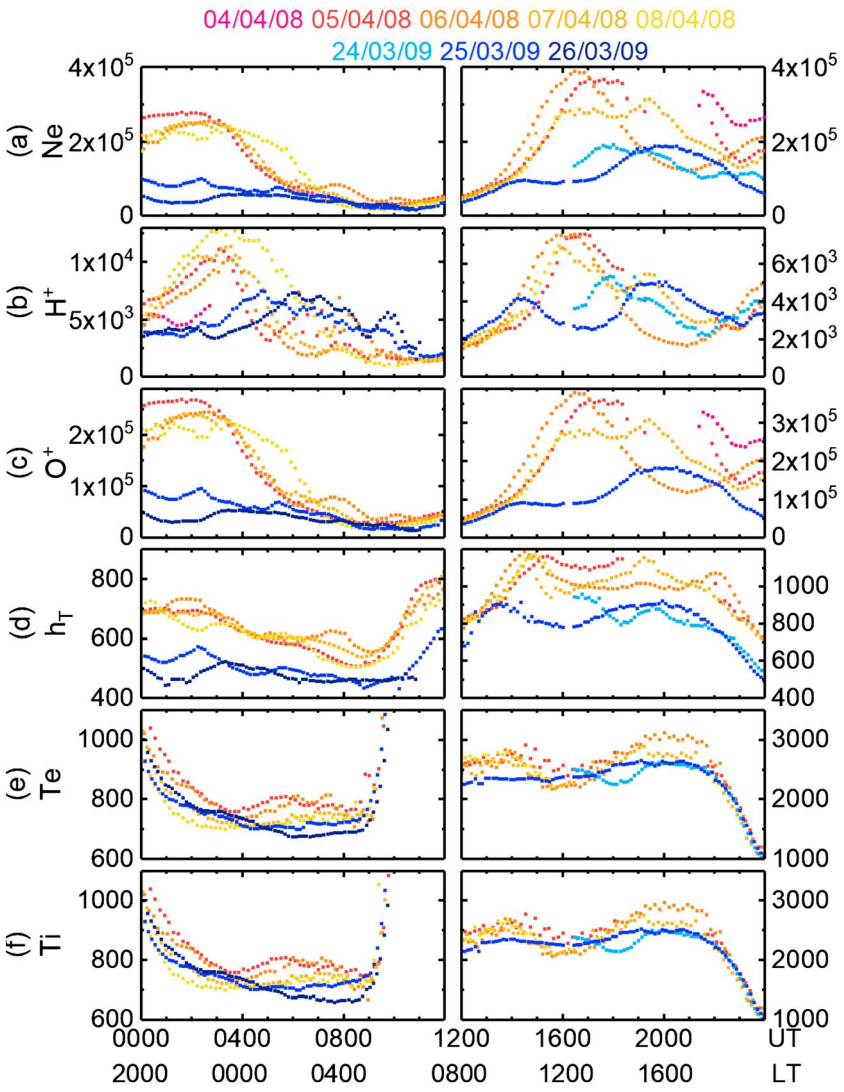

Figure 3. Comparison between the HSS (4–8 April 2008) and non-HSS (24–26 March 2009) intervals. From top to bottom, the panels show (a) Ne (cm^{-3}), (b) H^+, and (c) O^+ concentrations (cm^{-3}) at 400 km altitude, (d) h_T (km), (e) T_e (K), and (f) T_i (K) at h_T. Different colors correspond to different dates shown on the top. The UT and LT are shown at the bottom.

suggested to be cooler and contracted compared to those during previous solar minima [see *Heelis et al.*, 2009; *Coley et al.*, 2010; *Emmert et al.*, 2010; *Yue et al.*, 2010; *Klenzing et al.*, 2011; *Solomon et al.*, 2011; *Aponte et al.*, 2013, and references therein]. The variations of O^+/H^+ transition altitude, electron and ion temperatures, and densities estimated on a non-HSS period in the present work are consistent with the previous results. On the contrary, there is no study on the topside ionosphere response to a HSS during this interval that we know of.

The present study reveals that the topside ionosphere over Arecibo expanded in altitude and became hotter by the influence of the HSS. What is the source of this apparent ionospheric heating? At the present time we do not fully understand this. Arecibo is at a location where magnetospheric particle precipitation is not expected. There was not an intense magnetic storm (peak SYM-H was only −36 nT), so a storm dayside super-fountain effect [*Tsurutani et al.*, 2004, 2008; *Mannucci et al.*, 2005] is not expected. Large fluctuations in IMF B_z may create fluctuations in the prompt penetration electric fields during the substorms that occurred [e.g., *Nishida*, 1968; *Kelley et al.*, 1979]. This may possibly cause uplift of the ionosphere. Unfortunately, this cannot be verified as the plasma speed (or electric field) measurements by Arecibo radars were not available for the intervals in the study. However, since the location of Arecibo is so close to the magnetic equatorial region,

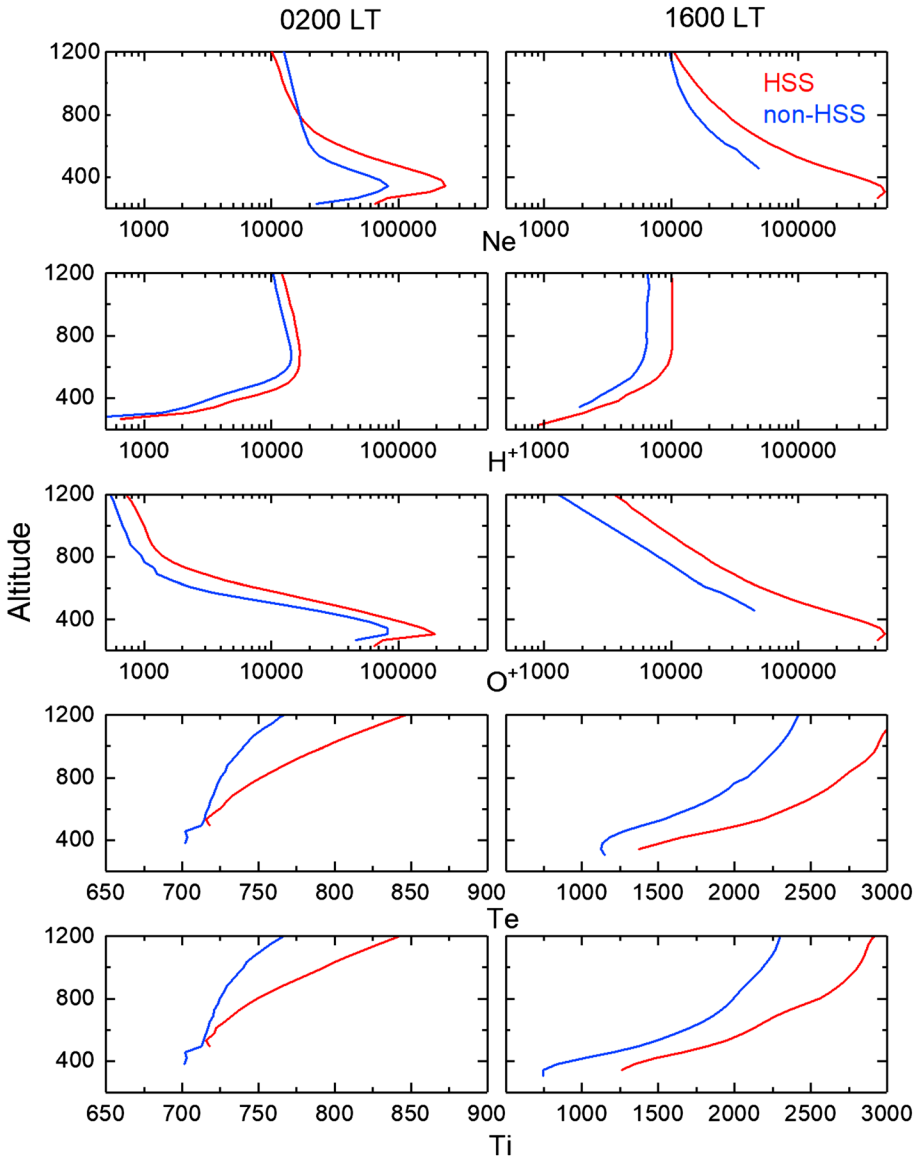

Figure 4. Average altitude profiles of Ne, H^+, O^+, T_e, and T_i, respectively, at local postmidnight (0200 LT) and afternoon (1600 LT). The red and blue plots pertain to HSS and non-HSS periods, respectively.

one has to consider a substorm superfountain as a possibility of the observed ionospheric uplift. Such a mechanism transports the plasma from the lower to higher altitude by upward $\mathbf{E} \times \mathbf{B}$ drift leading to plasma density increase in the *F* layer peak (see discussion in *Tsurutani et al*. [2008]). Relative enhancement of the *F* layer peak is clear from the altitude variations of the plasma density between the HSS and non-HSS days. Transport of the plasma content from lower apex height flux tubes to those at higher apex height results in dramatic plasma reduction in the plasmasphere. This is because the higher flux tubes have larger volumes. The topside electron temperature will increase due to the dramatic decrease in the electron cooling rate during the HSS event. One has basically the same amount of plasma occupying a larger volume, thus a lower plasma density. The input energy for heating is the same photoelectron heating, while the electron cooling rate decreases. The electron temperature gradient observed in the present study could be explained by a downward heat flux that heats the low altitude electrons.

Other possible ionospheric plasma heating mechanisms may be related to the plasmaspheric wave activity. We note that plasmaspheric hiss is significantly enhanced at $L = 1.1$ and variable between $L = 1.2$ and 2.0 during substorms [*Tsurutani et al*., 1975]. These electromagnetic waves were detected by a low-altitude satellite

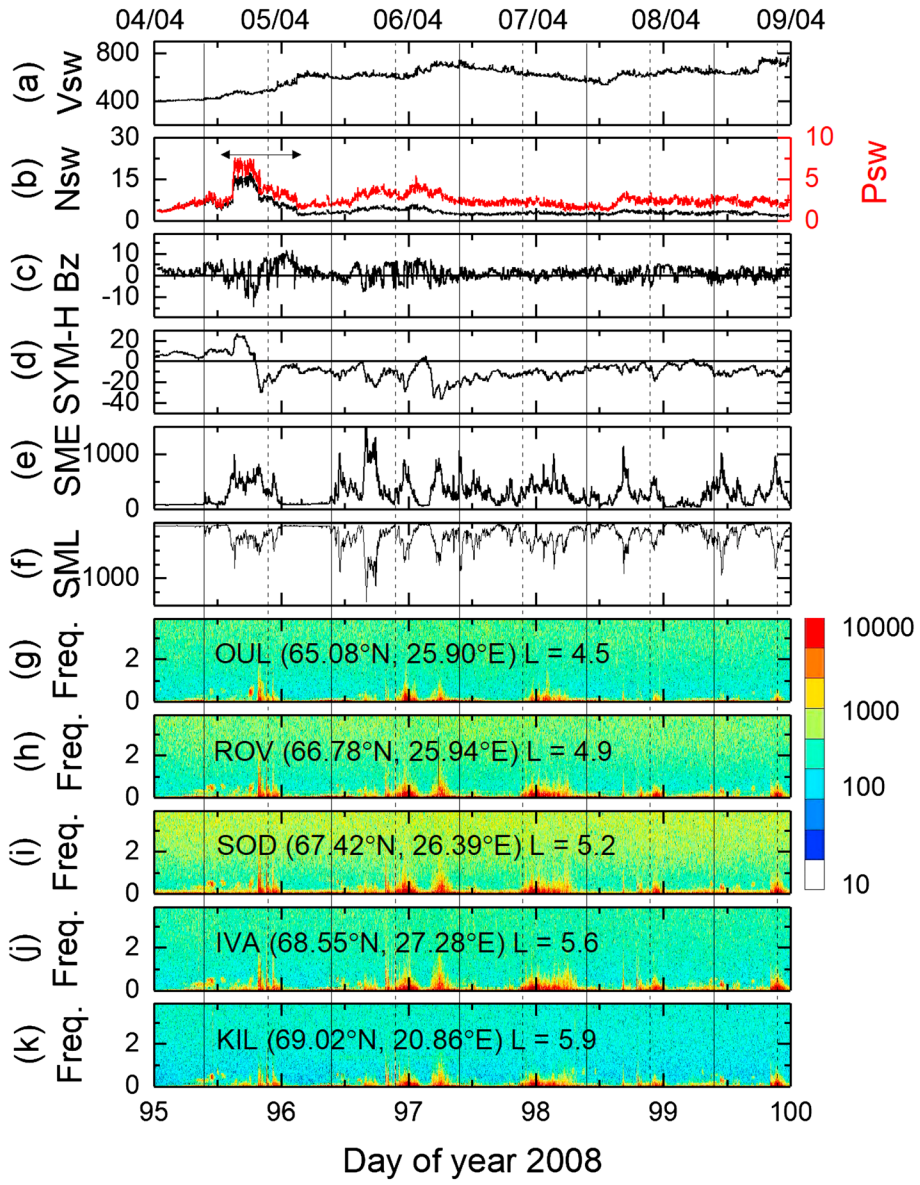

Figure 5. Pulsation magnetometer observations from Finnish ground magnetometer chain during the HSS event on 4–8 April 2008. From top to bottom, the panels show (a) V_{sw} (km s^{-1}), (b) N_{sw} (cm^{-3}, black) and P_{sw} (nPa, red), (c) IMF B_z (nT), (d) *SYM-H* (nT), (e) *SME* (nT), (f) *SML* (nT), and geomagnetic pulsations (in Hz) at (g) Oulu (OUL), (h) Rovaniemi (ROV), (i) Sodankylä (SOD), (j) Ivalo (IVA), and (k) Kilpisjärvi (KIL). The wave power in an arbitrary unit is shown by the color scale on the right. The geographic latitude, longitude, and *L* values of the observatories are shown in the panels. The vertical dashed and solid lines show the Finnish local midnight and noon in the unit of magnetic local time (MLT).

just above the ionosphere. Simple calculations indicate that Landau damping of these electromagnetic waves could resonate with and energize $E \sim 10$–100 eV electrons. These precipitating electrons could be a heat source for the topside ionosphere.

We also consider a third possible scenario for the observations, involving heating of thermal electrons by EMIC (electromagnetic ion cyclotron) waves. The southward IMF B_z component of the Alfvén waves within the HSS event causes substorms and injection events [*Tsurutani et al.*, 2004, 2016; *Hajra et al.*, 2014, 2015a, 2015b] causing the injection of energetic ~10–100 keV ions (and electrons) into the nightside outer zone magnetosphere. The substorm activity is indicated by the *SML* events shown in Figure 5f. The ions will gradient drift from midnight through dusk to local noon. The anisotropic ions will lead to the generation of EMIC

waves [*Cornwall*, 1965; *Kennel and Petschek*, 1966] as detected by the Finnish ground magnetometers (Figures 5g–5k). There is a second source of EMIC waves. The dayside compression of the outer magnetosphere by the HSS will lead to the compression of preexisting ~10–100 keV ions and dayside EMIC waves near local noon will also be generated [*Tsurutani et al*., 2001, 2016; *Remya et al*., 2014]. Thus, we can expect EMIC waves to be generated from local midnight through dusk to postnoon. This matches the EMIC wave local time distribution shown in Figures 5g–5k.

However, we note that the Finnish observatories (L ~ 4.5–5.9) exhibiting EMIC waves are far from the latitude of Arecibo (L = 1.3). How can waves generated at such high L reach Arecibo latitudes? Ray tracing studies applied to electromagnetic whistler mode waves called chorus [*Santolik et al*., 2003, 2004; *Bortnik et al*., 2009] may give us a clue. It has been shown that chorus generated in the outer zone magnetosphere can propagate to the plasmapause at high magnetic latitudes and enter the plasmasphere there. The chorus becomes plasmaspheric hiss and can propagate to low L shells. This scenario has been verified by *Falkowski et al*. [2017] who have shown that plasmaspheric hiss can reach L = 2 to 3 and farther earthward in the magnetosphere (see above description). These inner zone waves do not necessarily reach the ground. Can EMIC waves also propagate from the outer magnetosphere to the inner magnetosphere? If the EMIC waves can enter and reach low L, Landau damping of the EMIC waves may also be a possible solution.

The above latter two scenarios are consistent with and can explain the dramatic precipitation of low energy eV to keV electrons from the inner magnetosphere to the ionosphere associated with storm time substorms noted by the very interesting work of *Shiokawa et al*. [1996, 1997]. We urge scientists to study the propagation of both wave modes into the near-equatorial region of magnetosphere to better understand which scenario is the most likely mechanism.

Acknowledgments

The work of R.H. was supported by ANR under the financial agreement ANR-15-CE31-0009-01 at LPC2E/CNRS. Portions of this research were performed at the Jet Propulsion Laboratory, California Institute of Technology, under contract with NASA. E.E. would like to thank the Brazilian Federal Research Foundation (CNPq 302583/2015-7) agency for financial support. The Arecibo Observatory is operated by SRI International under a cooperative agreement with the NSF (AST-1100968) and in alliance with Ana G. Méndez-Universidad Metropolitana (UMET) and the Universities Space Research Association (USRA). The AO ionospheric data are available at Madrigal database (http://madrigal.naic.edu/madrigal/). $F_{10.7}$ solar fluxes were obtained from http://www.drao.nrc.ca/icarus. The solar wind/interplanetary data at ~1 AU are obtained from the OMNI database (http://omniweb.gsfc.nasa.gov/). The symmetric ring current index *SYM-H* is obtained from the World Data Center for Geomagnetism, Kyoto, Japan (http://wdc.kugi.kyoto-u.ac.jp/). The geomagnetic *SME* and *SML* indices are collected from the SuperMAG website (http://supermag.jhuapl.edu/). The magnetic pulsations at the Finnish observatory chain are obtained from http://www.sgo.fi/Data/archive.php. We wish to thank the two reviewers for extremely helpful and constructive comments. These helped improve our paper greatly.

References

Akasofu, S. I. (1964), The development of the auroral substorm, *Planet. Space Sci.*, *12*, 273–282, doi:10.1016/0032-0633(64)90151-5.

Antonova, L. A., V. A. Ershova, G. S. Ivanov-Kholodnyi, and V. G. Istomin (1992), Height of the transition from $O(^+)$ ions to $H(^+)$ ions according to Aktivnyi-satellite data and the dependence of this height on solar activity, *Geomag. Aeron.*, *32*, 59–63.

Aponte, N., C. G. M. Brum, M. P. Sulzer, and S. A. González (2013), Measurements of the O^+ to H^+ transition height and ion temperatures in the lower topside ionosphere over Arecibo for equinox conditions during the 2008–2009 extreme solar minimum, *J. Geophys. Res. Space Physics*, *118*, 4465–4470, doi:10.1002/jgra.50416.

Belcher, J. W., and L. Davis Jr. (1971), Large-amplitude Alfvén waves in the interplanetary medium: 2, *J. Geophys. Res.*, *76*, 3534–3563, doi:10.1029/JA076i016p03534.

Bortnik, J., W. Li, R. M. Thorne, V. Angelopoulos, C. Cully, J. Bonnell, O. Le Contel, and A. Roux (2009), An observation linking the origin of plasmaspheric hiss to discrete chorus emissions, *Science*, *324*, 775–778.

Coley, W. R., R. A. Heelis, M. R. Hairston, G. D. Earle, M. D. Perdue, R. A. Power, L. L. Harmon, B. J. Holt, and C. R. Lippincott (2010), Ion temperature and density relationships measured by CINDI from the C/NOFS spacecraft during solar minimum, *J. Geophys. Res.*, *115*, A02313, doi:10.1029/2009JA014665.

Cornwall, J. M. (1965), Cyclotron instabilities and electromagnetic emission in the ultra low frequency and very low frequency ranges, *J. Geophys. Res.*, *70*, 61–69, doi:10.1029/JZ070i001p00061.

DeForest, S. E., and C. E. McIlwain (1971), Plasma clouds in the magnetosphere, *J. Geophys. Res.*, *76*, 3587–3611, doi:10.1029/JA076i016p03587.

de Toma, G. (2010), Evolution of coronal holes and implications for high-speed solar wind during the minimum between cycles 23 and 24, *Sol. Phys.*, *274*, 195–217, doi:10.1007/s11207-010-9677-2.

de Toma, G. (2012), Polar magnetic fields and coronal holes during the recent solar minima, *Proc. Int. Astron. Union*, *286*, 101–112, doi:10.1017/S1743921312004711.

Dungey, J. W. (1961), Interplanetary magnetic field and the auroral zones, *Phys. Rev. Lett.*, *6*, 47–48.

Echer, E., B. T. Tsurutani, W. D. Gonzalez, and J. U. Kozyra (2011), High speed stream properties and related geomagnetic activity during the Whole Heliosphere Interval (WHI): 20 March to 16 April 2008, *Sol. Phys.*, *274*, 303–320, doi:10.1007/s11207-011-9739-0.

Echer, E., B. T. Tsurutani, and W. D. Gonzalez (2012), Extremely low geomagnetic activity during the recent deep solar cycle minimum, *Proc. Int. Astron. Union*, *7*, 200–209, doi:10.1017/S174392131200484X.

Emmert, J. T., J. L. Lean, and J. M. Picone (2010), Record-low thermospheric density during the 2008 solar minimum, *Geophys. Res. Lett.*, *37*, L12102, doi:10.1029/2010GL043671.

Falkowski, B. J., B. T. Tsurutani, G. S. Lakhina, and J. S. Pickett (2017), Two sources of dayside intense, quasi-coherent plasmaspheric hiss: A new mechanism for the slot region?, *J. Geophys. Res. Space Physics*, *122*, 1643–1657, doi:10.1002/2016JA023289.

Farley, D. T. (1970), Incoherent scattering at radio frequencies, *J. Atmos. Terr. Phys.*, *32*, 693–704.

Garzón, D. P., C. G. M. Brum, E. Echer, N. Aponte, M. P. Sulzer, S. A. González, R. B. Kerr, and L. Waldrop (2011), Response of the topside ionosphere over Arecibo to a moderate geomagnetic storm, *J. Atmos. Terr. Phys.*, *73*, 1568–1574, doi:10.1016/j.jastp.2011.02.016.

Gjerloev, J. W. (2009), A global ground-based magnetometer initiative, *Eos Trans. AGU*, *90*, 230–231, doi:10.1029/2009EO270002.

Gonzalez, W. D., J. A. Joselyn, Y. Kamide, H. W. Kroehl, G. Rostoker, B. T. Tsurutani, and V. M. Vasyliunas (1994), What is a geomagnetic storm?, *J. Geophys. Res.*, *99*, 5771–5792.

González, S. A., and M. P. Sulzer (1996), Detection of He^+ layering in the topside ionosphere over Arecibo during equinox solar minimum conditions, *Geophys. Res. Lett.*, *23*, 2509–2512, doi:10.1029/96GL02212.

González, S. A., M. P. Sulzer, M. J. Nicolls, and R. B. Kerr (2004), Solar cycle variability of nighttime topside helium ion concentrations over Arecibo, *J. Geophys. Res.*, *109*, AO7302, doi:10.1029/2003JA010100.

Gordon, W. E. (1964), Arecibo ionospheric observatory: Studies of the upper atmosphere and planets are made with the aid of a huge reflector in Puerto Rico, *Science*, *146*, 26–30.

Hajra, R., E. Echer, B. T. Tsurutani, and W. D. Gonzalez (2013), Solar cycle dependence of High-Intensity Long-Duration Continuous AE Activity (HILDCAA) events, relativistic electron predictors?, *J. Geophys. Res. Space Physics*, *118*, 5626–5638, doi:10.1002/jgra.50530.

Hajra, R., B. T. Tsurutani, E. Echer, and W. D. Gonzalez (2014), Relativistic electron acceleration during high-intensity, long-duration, continuous AE activity (HILDCAA) events: Solar cycle phase dependences, *Geophys. Res. Lett.*, *41*, 1876–1881, doi:10.1002/2014GL059383.

Hajra, R., B. T. Tsurutani, E. Echer, W. D. Gonzalez, and O. Santolik (2015a), Relativistic ($E > 0.6$, > 2.0, and > 4.0 MeV) electron acceleration at geosynchronous orbit during high-intensity, long-duration, continuous ae activity (HILDCAA) events, *Astrophys. J.*, *799*, 39, doi:10.1088/0004-637X/799/1/39.

Hajra, R., B. T. Tsurutani, E. Echer, W. D. Gonzalez, C. G. M. Brum, L. E. A. Vieira, and O. Santolik (2015b), Relativistic electron acceleration during HILDCAA events: Are precursor CIR magnetic storms important?, *Earth Planets Space*, *67*, 109, doi:10.1186/s40623-015-0280-5.

Hajra, R., B. T. Tsurutani, E. Echer, W. D. Gonzalez, and J. W. Gjerloev (2016), Supersubstorms (SML < -2500 nT): Magnetic storm and solar cycle dependences, *J. Geophys. Res. Space Physics*, *121*, 7805–7816, doi:10.1002/2015JA021835.

Heelis, R. A., and W. B. Hanson (1980), Interhemispheric transport induced by neutral zonal winds in the F region, *J. Geophys. Res.*, *85*, 3045–3047, doi:10.1029/JA085iA06p03045.

Heelis, R. A., W. R. Coley, A. G. Burrell, M. R. Hairston, G. D. Earle, M. D. Perdue, R. A. Power, L. L. Harmon, B. J. Holt, and C. R. Lippincott (2009), Behavior of the O+/H+ transition height during the extreme solar minimum of 2008, *Geophys. Res. Lett.*, *36*, L00C03, doi:10.1029/2009GL038652.

Horne, R. B., and R. M. Thorne (1998), Potential waves for relativistic electron scattering and stochastic acceleration during magnetic storms, *Geophys. Res. Lett.*, *25*, 3011–3014, doi:10.1029/98GL01002.

Kelley, M. C., B. G. Fejer, and C. A. Gonzales (1979), An explanation for anomalous equatorial ionospheric electric fields associated with a northward turning of the interplanetary magnetic field, *Geophys. Res. Lett.*, *6*, 301–304.

Kennel, C. F., and H. E. Petschek (1966), Limit on stably trapped particle fluxes, *J. Geophys. Res.*, *71*, 1–28.

Klenzing, J., F. Simões, S. Ivanov, R. A. Heelis, D. Bilitza, R. Pfaff, and D. Rowland (2011), Topside equatorial ionospheric density and composition during and after extreme solar minimum, *J. Geophys. Res.*, *116*, A12330, doi:10.1029/2011JA017213.

Kotov, D. V., V. Truhlík, P. G. Richards, S. Stankov, O. V. Bogomaz, L. F. Chernogor, and I. F. Domnin (2015), Night-time light ion transition height behaviour over the Kharkiv (50°N, 36°E) IS radar during the equinoxes of 2006–2010, *J. Atmos. Sol. Terr. Phys.*, *132*, 1–12.

Krieger, A. S., A. F. Timothy, and E. C. Roelof (1973), A coronal hole and its identification as the source of a high velocity solar wind stream, *Sol. Phys.*, *29*, 505–525.

MacPherson, B., S. A. González, G. J. Bailey, R. J. Moffett, and M. P. Sulzer (1998), The effects of meridional neutral winds on the O^+-H^+ transition altitude over Arecibo, *J. Geophys. Res.*, *103*, 29,183–29,198, doi:10.1029/98JA02660.

Mannucci, A. J., B. T. Tsurutani, B. A. Iijima, A. Komjathy, A. Saito, W. D. Gonzalez, F. L. Guarnieri, J. U. Kozyra, and R. Skoug (2005), Dayside global ionospheric response to the major interplanetary events of October 29–30, 2003 "Halloween Storms", *Geophys. Res. Lett.*, *32*, L12S02, doi:10.1029/2004GL021467.

Miyazaki, S. (1979), Ion transition height distribution obtained with the satellite Taiyo, *J. Geomagn. Geoelec.*, *31*, S113–S124.

Newell, P. T., and J. W. Gjerloev (2011), Evaluation of SuperMAG auroral electrojet indices as indicators of substorms and auroral power, *J. Geophys. Res.*, *116*, A12211, doi:10.1029/2011JA016779.

Nishida, A. (1968), Coherence of geomagnetic DP 2 fluctuations with interplanetary magnetic variations, *J. Geophys. Res.*, *73*, 5549–5559.

Remya, B., B. T. Tsurutani, R. V. Reddy, G. S. Lakhina, B. J. Falkowski, E. Echer, and K. H. Glassmeier (2014), Large-amplitude, circularly polarized, compressive, obliquely propagating electromagnetic proton cyclotron waves throughout the Earth's magnetosheath: Low plasma β conditions, *Astrophys. J.*, *793*, 6, doi:10.1088/0004-637X/793/1/6.

Remya, B., B. T. Tsurutani, R. V. Reddy, G. S. Lakhina, and R. Hajra (2015), Electromagnetic cyclotron waves in the dayside subsolar outer magnetosphere generated by enhanced solar wind pressure: EMIC wave coherency, *J. Geophys. Res. Space Physics*, *120*, 7536–7551, doi:10.1002/2015JA021327.

Remya, B., K. H. Lee, L. C. Lee, and B. T. Tsurutani (2017), Coherency and ellipticity of electromagnetic ion cyclotron waves: Satellite observations and simulations, *J. Geophys. Res. Space Physics*, *122*, 3374–3396, doi:10.1002/2016JA023588.

Rostoker, G., S.-I. Akasofu, J. Foster, R. A. Greenwanild, Y. Kamide, K. Kawasaki, A. T. Y. Lui, R. L. McPherron, and C. T. Russell (1980), Magnetospheric substorms—Definition and signatures, *J. Geophys. Res.*, *85*, 1663–1668, doi:10.1029/JA085iA04p01663.

Santolik, O., D. A. Gurnett, J. S. Pickett, M. Parrot, and N. Cornilleau-Wehrlin (2003), Spatio-temporal structure of storm-time chorus, *J. Geophys. Res.*, *108*(A7), 1278, doi:10.1029/2002JA009791.

Santolik, O., D. A. Gurnett, and J. S. Pickett (2004), Multipoint investigation of the source region of storm-time chorus, *Ann. Geophys.*, *22*, 2555–2563.

Sheeley, N. R., Jr., J. W. Harvey, and W. C. Feldman (1976), Coronal holes, solar wind streams and recurrent geomagnetic disturbances: 1973–1976, *Sol. Phys.*, *49*, 271–278.

Shiokawa, K., K. Yumoto, C. I. Meng, and G. Reeves (1996), Broadband electrons observed by the DMSP satellites during storm-time substorms, *Geophys. Res. Lett.*, *23*, 2529–2532.

Shiokawa, K., C.-I. Meng, G. D. Reeves, F. J. Rich, and K. Yumoto (1997), A multievent study of broadband electrons observed by the DMSP satellites and their relation to red aurora observed at midlatitude stations, *J. Geophys. Res.*, *102*, 14,237–14,253.

Smith, E. J., and J. H. Wolfe (1976), Observations of interaction regions and corotating shocks between one and five AU: Pioneers 10 and 11, *Geophys. Res. Lett.*, *3*, 137–140, doi:10.1029/GL003i003p00137.

Solomon, S. C., L. Qian, L. V. Didkovsky, R. A. Viereck, and T. N. Woods (2011), Causes of low thermospheric density during the 2007–2009 solar minimum, *J. Geophys. Res.*, *116*, A00H07, doi:10.1029/2011JA016508.

Titheridge, J. E. (1976), Ion transition heights from topside electron density profiles, *Planet. Space Sci.*, *24*, 229–245.

Tsurutani, B. T., and W. D. Gonzalez (1987), The cause of high-intensity long-duration continuous *AE* activity (HILDCAAs): Interplanetary Alfvén wave trains, *Planet. Space Sci.*, *35*, 405–412.

Tsurutani, B. T., E. J. Smith, and R. M. Thorne (1975), Electromagnetic hiss and relativistic electron losses in the inner zone, *J. Geophys. Res.*, *80*, 600–607.

Tsurutani, B. T., C. M. Ho, E. J. Smith, M. Neugebauer, B. E. Goldstein, J. S. Mok, J. K. Arballo, A. Balogh, D. J. Southwood, and W. C. Feldman (1994), The relationship between interplanetary discontinuities and Alfvén waves: Ulysses observations, *Geophys. Res. Lett.*, *21*, 2267–2270.

Tsurutani, B. T., W. D. Gonzalez, A. L. C. Gonzalez, F. Tang, J. K. Arballo, and M. Okada (1995), Interplanetary origin of geomagnetic activity in the declining phase of the solar cycle, *J. Geophys. Res.*, *100*, 21,717–21,733, doi:10.1029/95JA01476.

Tsurutani, B. T., X. Y. Zhou, V. M. Vasyliunas, G. Haerendel, J. K. Arballo, and G. S. Lakhina (2001), Interplanetary shocks, magnetopause boundary layers and dayside auroras: The importance of a very small magnetospheric region, *Surv. Geophys.*, *22*, 101–130.

Tsurutani, B. T., W. D. Gonzalez, F. Guarnieri, Y. Kamide, X. Zhou, and J. K. Arballo (2004), Are high-intensity long-duration continuous AE activity (HILDCAA) events substorm expansion events?, *J. Atmos. Sol. Terr. Phys.*, *66*, 167–176.

Tsurutani, B. T., E. Echer, F. L. Guarnieri, and J. U. Kozyra (2008), CAWSES November 7–8, 2004 superstorm: Complex solar and interplanetary features in the post-solar maximum phase, *Geophys. Res. Lett.*, *35*, L06S05, doi:10.1029/2007GL031473.

Tsurutani, B. T., E. Echer, and W. D. Gonzalez (2011), The solar and interplanetary causes of the recent minimum in geomagnetic activity (MGA23): A combination of midlatitude small coronal holes, low IMF B_z variances, low solar wind speeds and low solar magnetic fields, *Ann. Geophys.*, *29*, 839–849.

Tsurutani, B. T., R. Hajra, E. Echer, and J. W. Gjerloev (2015), Extremely intense (SML ≤ -2500 nT) substorms: Isolated events that are externally triggered?, *Ann. Geophys. Comm.*, *33*, 519–524, doi:10.5194/angeocom-33-519-2015.

Tsurutani, B. T., et al. (2016), Heliospheric plasma sheet (HPS) impingement onto the magnetosphere as a cause of relativistic electron dropouts (REDs) via coherent EMIC wave scattering with possible consequences for climate change mechanisms, *J. Geophys. Res. Space Physics*, *121*, 10,130–10,156, doi:10.1002/2016JA022499.

Yue, X., W. S. Schreiner, J. Lei, C. Rocken, Y. Kuo, and W. Wan (2010), Climatology of ionospheric upper transition height derived from COSMIC satellites during the solar minimum of 2008, *J. Atmos. Terr. Phys.*, *72*, 1270–1274, doi:10.1016/j.jastp.2010.08.018.